1-2013

A Remotely Sensed Global Terrestrial Drought Severity Index

Qiaozhen Mu

Maosheng Zhao

John S. Kimball
University of Montana - Missoula

Nate McDowell

Steven W. Running
University of Montana - Missoula

Recommended Citation

Mu, Q., M. Zhao, J. Kimball, N. McDowell, and S. Running, 2013: A Remotely Sensed Global Terrestrial Drought Severity Index. Bull. Amer. Meteor. Soc., 94, 83–98, doi: 10.1175/BAMS-D-11-00213.1

Volume 94 Number 1 January 2013

BAMS

Bulletin of the American Meteorological Society

SEAMLESS PREDICTION

GET READY FOR PYTHON

A DECADE OF OSIRIS

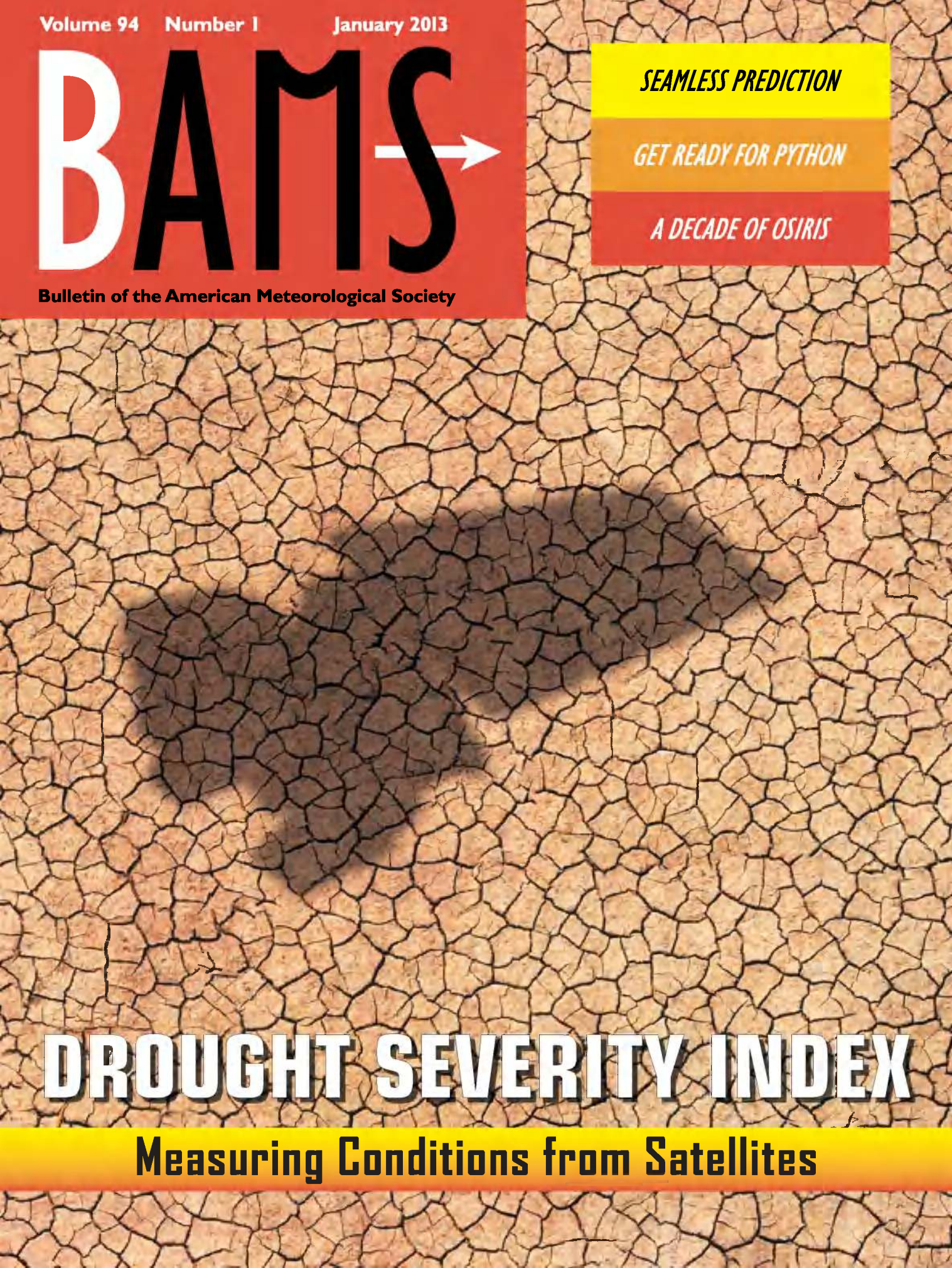

DROUGHT SEVERITY INDEX

Measuring Conditions from Satellites

A REMOTELY SENSED GLOBAL TERRESTRIAL DROUGHT SEVERITY INDEX

BY QIAOZHEN MU, MAOSHENG ZHAO, JOHN S. KIMBALL, NATHAN G. MCDOWELL, AND STEVEN W. RUNNING

A new global index uses operational satellite remote sensing as primary inputs and enhances near real-time drought monitoring and mitigation efforts.

Water is essential for life. With increasing human development and climate change, water has become a pivotal resource for sustainable development, both societally and environmentally. Agriculture, on which a burgeoning population depends for food, is competing with industrial, household, and environmental uses for increasingly scarce freshwater supplies in many areas (Vörösmarty et al. 2010; Rosegrant et al. 2003). Drought is an important adverse climatic event for both ecosystems and human society. Global mean surface air temperature has increased by about 0.76°C since 1850 (Trenberth et al. 2007) and is expected to increase by 1.5°–6.4°C by the end of the twenty-first century (Meehl et al. 2007). Under a warming climate, persistent drought may increase (Dai et al. 2004; Pachauri and Reisinger 2007; Dai 2011b), while human populations and associated demands for freshwater resources are rising, increasing food production constraints and putting global food security at risk. Accurate and consistent global mapping and monitoring of drought severity is essential for water management and drought mitigation efforts.

AFFILIATIONS: MU, ZHAO, AND RUNNING—Numerical Terradynamic Simulation Group, College of Forestry and Conservation, University of Montana, Missoula, Montana; KIMBALL—Flathead Lake Biological Station, University of Montana, Polson, Montana; MCDOWELL—Earth and Environmental Sciences, Atmospheric and Environmental Dynamics Group, Los Alamos National Laboratory, Los Alamos, New Mexico
CORRESPONDING AUTHOR: Qiaozhen Mu, Numerical Terradynamic Simulation Group, College of Forestry and Conservation, University of Montana, 32 Campus Drive, Missoula, MT 59812
E-mail: qiaozhen@ntsg.umt.edu

The abstract for this article can be found in this issue, following the table of contents.
DOI:10.1175/BAMS-D-11-00213.1

In final form 10 April 2012

COMMON DROUGHT SEVERITY INDICES.

There are several indices used widely for regional- to global-scale drought assessment and monitoring. Drought indices integrate large amounts of data, such as precipitation, snowpack, streamflow, and other water supply indicators, to monitor drought severity in a comprehensive framework and to measure how much the climate in a given period has deviated from historically established normal conditions (Narasimhan and Srinivasan 2005). In this section, we give a brief review of some of the most widely used drought indices, including the Palmer drought severity index (PDSI; Palmer 1965; Alley 1984), U.S. Drought Monitor (USDM; Svoboda et al. 2002), and

a newly developed evaporative drought index (EDI) by Yao et al. (2010).

PDSI. Among widely used drought indices (Heim 2002), the PDSI (Palmer 1965; Alley 1984) is the only index that uses readily available monthly precipitation and temperature inputs to assess drought (Heim 2002). Palmer used a two-layer bucket model to quantify monthly water supply and demand by accounting for water inputs (precipitation), outputs (evaporation and runoff), and antecedent soil water status. The model also considers multiyear average monthly water exchanges so that for a given month, the departure level of precipitation (supply) from the normal water demand can be quantified. It is difficult to devise a universal drought index because of the spatial and temporal complexity of drought, and the limitations of the PDSI are well documented (Keyantash and Dracup 2002). The PDSI was originally developed to assess drought in semiarid climates, specifically, the Great Plains of the United States (Palmer 1965), and thus some parameters may not work well for other regions (Heim 2002; Keyantash and Dracup 2002). Some assumptions of the PDSI dealing with hydrological processes have also been criticized, such as not treating frozen soil or snow accumulation and melt processes, and actual evapotranspiration (ET) occurring at the potential rate (Dai et al. 2004; Heim 2002). Despite these limitations, Dai et al. (2004) found that the PDSI correlates with soil moisture during warm seasons.

To address some of the major PDSI constraints, several new variants of this approach have been developed, including the self-calibrating PDSI (Wells et al. 2004) and the PDSI using improved formulations for potential evapotranspiration (PET), such as the Penman–Monteith equation (Monteith 1965), instead of the original Thornthwaite equation (Thornthwaite 1948). Dai (2011a) compared and evaluated four forms of the PDSI over the 1850–2008 period and found that the four PDSI forms show similar long-term trends and correlations with observed monthly soil moisture, yearly streamflow, and satellite-observed water storage changes. Dai (2011a) suggested that other indices should be adopted to address limitations in the PDSI.

USDM. Currently, the National Oceanic and Atmospheric Administration (NOAA) and the U.S. Department of Agriculture (USDA) Foreign Agricultural Service (FAS) use the USDM (Svoboda et al. 2002; Lawrimore et al. 2002) to monitor vegetation drought stress in the United States (http://droughtmonitor.unl.edu/). The USDM assimilates several widely used climatic drought indices, including the PDSI (Palmer 1965), standardized precipitation index (SPI; McKee et al. 1993), percent of normal precipitation (PNP; Werick et al. 1994), land soil moisture and streamflow, satellite normalized difference vegetation index (NDVI), and many supplementary indicators for regional drought detection. However, in addition to the above-mentioned PDSI constraints and the limitations of other drought indices (Table 1), uncertainties in precipitation data (Gao et al. 2010) and heterogeneous soil moisture conditions may introduce large uncertainties for USDM drought detection and monitoring. Furthermore, the USDM only provides drought information across North America, and no ET data, which makes it less useful for operational water supply assessments. These assessments and the broader user community would benefit from consistent global drought severity index (DSI) and ET products at relatively fine (1-km resolution) spatial resolution approaching the optimal scale of utility for a wide range of water resource applications (Wood et al. 2011).

EDI. Yao et al. (2010) proposed an EDI to monitor droughts over the conterminous United States. They used Moderate Resolution Imaging Spectroradiometer (MODIS) and National Centers for Environmental Prediction–Department of Energy Atmospheric Model Intercomparison Project Reanalysis II (NCEP–DOE II) data, and statistical methods to estimate ET and PET at 4-km spatial resolution and a monthly time step, and used the deviation of the ET/PET ratio from unity to define the EDI. The integrated remote sensing data in the EDI are sensitive to the vegetation drought response and enhance EDI capabilities for drought monitoring and detection. However, the statistical models used to calculate ET and PET for the EDI calculation lack a physical basis, while the application of these models outside the domain and conditions from which they were developed can result in uncertain ET and PET estimates and degraded EDI accuracy. This limits the effective use of the EDI outside of the United States. The EDI also cannot easily quantify the wetness or dryness of a region in a given monthly or yearly period. For example, in a semiarid region where the ET/PET ratio is low, a small change in the ET/PET ratio might correspond to a significant change in wetness but result in missed drought detection. In contrast, for a wet region where the ET/PET ratio is high, a large change in EDI might not necessarily imply a significant change in water stress.

Table 1. Summary of the commonly used drought indices.

Indices	Description	Strengths	Weaknesses	Citations
PNP	A simple calculation by dividing the 30-yr average precipitation for the region, and multiplying by 100%.	Effective for a single region or season.	Precipitation does not have a normal distribution. PNP depends on location and season. PNP cannot identify specific drought impacts.	Werick et al. (1994)
Deciles	A simple calculation by grouping precipitation into deciles distributed from 1 to 10. The lowest value indicates conditions drier than normal and the higher value indicates conditions wetter than normal.	Accurate statistical measurement of drought response to precipitation, and providing uniformity in drought classifications.	Accurate calculations require a long climatology record of precipitation.	Gibbs and Maher (1967)
SPI	A simple calculation based on the concept that precipitation deficits over varying periods or time scales influence ground water, reservoir storage, soil moisture, snowpack, and streamflow.	Computed for flexible multiple time scales, provides early warning of drought and help assessing drought severity.	Precipitation is the only input data. SPI values based on long-term precipitation may change. The long time scale up to 24 months is not reliable.	McKee et al. (1993)
PDSI	Calculated using precipitation, temperature, and soil moisture data. Soil moisture algorithm has been calibrated for relatively homogeneous regions.	The first comprehensive drought index used widely to detect agricultural drought (see text for details).	PDSI may lag emerging droughts. Not effective for mountainous areas with frequent climatic extremes, or in winter and spring (see text for details).	Palmer (1965); Alley (1984)
PHDI	Derived from PDSI to quantify long-term impact from hydrological drought.	Same as PDSI, but more effective to determine when a drought ends.	PHDI may change more slowly than PDSI.	Palmer (1965)
CMI	A derivative of PDSI. CMI reflects moisture supply in the short term.	Effective for the detection of short-term agricultural drought sooner than PDSI.	CMI cannot monitor long-term droughts well.	Palmer (1968)
SWSI	Developed from the Palmer index by combining hydrological and climatic features.	SWSI takes into account reservoir storage, streamflow, snowpack, and precipitation. Effective under snowpack conditions.	SWSI is difficult to compare between different basins. SWSI cannot detect extreme events effectively. Not a suitable indicator for agricultural drought.	Shafer and Dezman (1982); Wilhite and Glantz (1985); Doesken et al. (1991)
RDI	Similar to SPI based on precipitation and PET.	Drought is based on both precipitation and PET. Appropriate for climate change scenarios.	Uncertainties in input data for the calculation of PET. RDI at different basins cannot be compared with each other and has been computed seasonally.	Tsakiris and Vangelis (2005); Tsakiris et al. (2007)
USDM	Based on several key physical indicators, such as PDSI, SPI, PNP, soil moisture model percentiles, daily streamflow percentiles, remotely sensed satellite vegetation health index, and many supplementary indicators.	Integrating remotely sensed satellite vegetation health index together with other drought indices (see text for details).	USDM is weighted to precipitation and soil moisture in short term. USDM inherits the weaknesses of the other indices it uses (see text for details).	Svoboda et al. (2002)

Other commonly used drought indices (Table 1) include PNP (Werick et al. 1994), deciles (Gibbs and Maher 1967), SPI (McKee et al. 1993), the Palmer hydrological drought index (PHDI; Palmer 1965), the crop moisture index (CMI; Palmer 1968), the surface water supply index (SWSI; Shafer and Dezman 1982; Wilhite and Glantz 1985; Doesken et al. 1991), and the reclamation drought index (RDI; Tsakiris and Vangelis 2005; Tsakiris et al. 2007). The relative strengths and weaknesses of these indices are summarized in Table 1, while most were designed to detect meteorological and/or hydrological drought without incorporating vegetation responses into drought.

To overcome these limitations and to exploit the relative wealth of operational satellite records and associated vegetation indicators, we developed a DSI algorithm using satellite-derived ET, PET, and NDVI products to detect and monitor droughts on a global basis. Precipitation and soil moisture are not used as DSI algorithm inputs because of current large spatial uncertainties in these data.

REMOTELY SENSED GLOBAL DSI. The strengths of remotely sensed data, especially those from polar-orbiting satellites, are to provide temporally and spatially continuous information over vegetated surfaces useful for monitoring surface biophysical variables affecting ET, including albedo, biome type, and leaf area index (LAI; Los et al. 2000). MODIS on board the National Aeronautics and Space Administration's (NASA's) *Terra* and *Aqua* satellites provides unprecedented information on vegetation and surface energy conditions (Justice et al. 2002). Despite the strengths in the models and concepts of the various drought indices summarized in Table 1, except for the USDM and EDI, which use both reanalysis meteorological data and remotely sensed data (Svoboda et al. 2002; Yao et al. 2010), most drought indices use reanalysis meteorological data that contain substantial uncertainties (Zhao et al. 2006; Chen and Bosilovich 2007; Gao et al. 2010). Mu et al. (2007, 2009, 2011b) developed a MODIS ET model to estimate ET and PET using MODIS data. Using the MODIS ET/PET (Mu et al. 2007, 2009, 2011b) and MODIS NDVI (Huete et al. 2002) data products, we calculated the remotely sensed DSI globally for all vegetated land areas at 8-day, monthly, and annual intervals over the MODIS (collection 5) operational record from 2000 to 2011.

In the following sections, we first introduce the input datasets and the DSI model; we then evaluate DSI patterns and anomalies in relation to alternative global PDSI information and documented regional drought events. The MODIS operational net primary production (NPP) product is used as an indicator of vegetation productivity changes under documented severe droughts in the Amazon, Europe, and Russia, and to evaluate corresponding DSI- and PDSI-based vegetation drought responses. Finally, we discuss the DSI sensitivity and uncertainties in relation to different base periods and input data.

Datasets. Operational global land products available from MODIS on NASA Earth Observing System (EOS) *Terra* and *Aqua* satellites include the MOD16 ET/PET (Mu et al. 2007, 2009, 2011b) products and provide a means to quantify water fluxes between terrestrial ecosystems and the atmosphere. The MOD16 ET and PET data are used as primary inputs to calculate the DSI on a global basis for all terrestrial ecosystems at continuous 8-day, monthly, and annual time steps and 1-km spatial resolution. Daily meteorological reanalysis data and 8-day remotely sensed vegetation property dynamics from MODIS are used as inputs to the MOD16 ET/PET algorithm.

The MOD16 ET/PET algorithm uses the well-known Penman–Monteith equation (P-M) (Monteith 1965) to calculate global remotely sensed ET (Mu et al. 2007, 2009, 2011b), and integrates both P-M (Monteith 1965) and Priestley-Taylor (1972) methods to estimate PET (Mu et al. 2007, 2011b). The ET algorithm accounts for both surface energy partitioning and environmental constraints on ET, and includes evaporation from canopy interception, wet and moist soil surfaces, and transpiration from canopy stomata. Atmosphere relative humidity is used to quantify the proportion of wet soil and wet canopy components (Fisher et al. 2008). Proportional vegetation cover is estimated from MODIS fraction of photosynthetically active radiation (FPAR) retrievals (Los et al. 2000), and used to partition net radiation between vegetation and soil surfaces. Leaf-level stomatal conductance is controlled by the average daytime surface air vapor pressure deficit (VPD) and daily minimum air temperature, and is further upscaled to the canopy level that is not covered by water using MODIS (MOD15) LAI (Myneni et al. 2002). Using the complementary relationship hypothesis (Bouchet 1963; Fisher et al. 2008), soil evaporation is estimated as the potential evaporation rate for wet soil surfaces scaled down by relative humidity and VPD for moist soil conditions. The daily ET calculation represents the sum of daytime and nighttime ET estimates. Additional details regarding the MODIS ET/PET algorithm logic and accuracy are described elsewhere (Mu et al. 2007, 2011b).

The MODIS (MOD16) global ET product has been widely validated (Mu et al. 2011b) and applied for regional and global analyses (e.g., Montenegro et al. 2009; Jung et al. 2010; Loarie et al. 2011). The ET product shows generally favorable correspondence ($r = 0.86$, statistical significance $p < 0.0001$) with daily ET estimates based on tower eddy covariance measurements for a wide range of global land cover and climate conditions (Mu et al. 2011b). The mean absolute error of the MODIS ET retrievals was found to be approximately 24.1% of the average measured ET, and within the range (10%–30%) of ET measurement uncertainty (Courault et al. 2005; Jiang et al. 2004; Kalma et al. 2008; Mu et al. 2011b). The MODIS ET estimates were also found to account for approximately 85% of the global variability in ET estimates based on river discharge measurements from 232 global watersheds (Q. Mu et al. 2012, unpublished manuscript). A global analysis of MODIS ET retrievals from 2000 to 2010 indicate a total annual ET flux from the vegetated land surface of 63.4×10^3 km^3, with an average of 569 ± 358 mm yr^{-1}, similar to the previously reported annual ET estimate of 65.5×10^3 km^3 for the global land surface (Oki and Kanae 2006).

Satellite vegetation greenness indices (VIs), especially the NDVI and enhanced vegetation index (EVI), have been successfully used to monitor global vegetation photosynthetic activity (Tucker 1979; Justice et al. 2002; Huete et al. 2002). The VIs can potentially link climate changes (e.g., increasing frequency and severity of drought) and vegetation responses as observed through vegetation greenness changes with land–atmosphere water, carbon and energy fluxes, and associated climate feedbacks (Atkinson et al. 2011). We integrate the operational MOD16 ET/PET and MOD13 NDVI products to calculate a new remotely sensed global DSI.

Methodology. ET is a metric of ecosystem functional status and is directly related to water, carbon, and energy cycles of the land surface. The ratio of ET to PET is commonly used as an indicator of terrestrial water availability and associated wetness or drought. For each 8-day, monthly, and annual composite period, we calculate the ratio of ET to PET (*Ratio*) as

$$Ratio = \frac{ET}{PET}. \tag{1}$$

The temporal standard deviation of Ratio (σ_{Ratio}) and Ratio average ($\overline{Ratio}$) are then computed on a gridcell-wise basis over the available satellite record (2000–present). The standardized Ratio (Z_{Ratio}) is then calculated as

$$Z_{\text{Ratio}} = \frac{Ratio - \overline{Ratio}}{\sigma_{\text{Ratio}}}. \tag{2}$$

We derive the standardized NDVI (Z_{NDVI}) for each composite period during the classified growing season at each grid cell as

$$Z_{\text{NDVI}} = \frac{NDVI - \overline{NDVI}}{\sigma_{\text{NDVI}}}. \tag{3}$$

The Z_{Ratio} and Z_{NDVI} terms are then summed as

$$Z = Z_{\text{Ratio}} + Z_{\text{NDVI}}. \tag{4}$$

The remotely sensed DSI is finally calculated as the standardized Z value as

$$DSI = \frac{z - \overline{z}}{\sigma_z}, \tag{5}$$

where the DSI is a dimensionless index ranging theoretically from unlimited negative values (drier than normal) to unlimited positive values (wetter than normal). Because of relative greater noise in the nongrowing-season NDVI signal (Zhao and Running 2011), we only use NDVI during the classified snow-free growing season indicated by the MODIS 8-day Climate Model Grid (CMG) 0.05° snow cover (MOD10C2; Hall and Riggs 2007); the DSI is derived using ET/PET without NDVI during the classified dormant season.

The DSI model uses relatively finescale (1-km resolution) NDVI inputs from MODIS, which provides potential advantages over other global drought indices. First, the MODIS (MOD15) LAI/FPAR product (Myneni et al. 2002) is produced at 8-day intervals and is a primary input to the MOD16 ET algorithm (Mu et al. 2011b), instead of the finer (250 m) resolution but coarser (16-day) temporal fidelity MOD13 NDVI/EVI product (Huete et al. 2002); the MOD15 and MOD13 products are derived independently using the same atmosphere-corrected surface reflectance data (Vermote and Kotchenova 2010) as inputs. The NDVI is also sensitive to vegetation drought response (Atkinson et al. 2011) and associated water stress, especially over water-limited regions (Paruelo et al. 1995; Schultz et al. 1995; Douglas et al. 1996; Nicholson et al. 1998). The MODIS ET/PET algorithm uses coarse-resolution global NCEP–DOE II (Kanamitsu et al. 2002) reanalysis data as daily metrological drivers, which, like all existing reanalysis datasets, contains

uncertainties, especially in the tropics (Zhao et al. 2006). Small-scale convection dominates atmospheric processes in the tropics and the convection scale is too small for coarse-resolution reanalysis systems to render in detail (Kerr 2011). Integrating the NDVI into the DSI calculation partially mitigates model uncertainties associated with the reanalysis inputs for improved DSI accuracy.

ANCILLARY DATA. Another operational global land product available from MODIS on the NASA EOS *Terra* and *Aqua* satellites, the MODIS (MOD17) product (Running et al. 2004; Zhao et al. 2005; Zhao and Running 2010), provides estimates of vegetation gross primary production (GPP) and net primary production (NPP) at consistent spatial and temporal resolutions for global vegetated land areas. The MOD17 GPP/NPP product has been widely validated and applied to regional and global scales (Turner et al. 2005, 2006; Heinsch et al. 2006; Zhao and Running 2010). The MOD17 GPP/NPP product was used in this study as a surrogate measure of vegetation activity and associated NPP response to severe droughts, for comparison against DSI and PDSI global patterns and temporal changes.

The widely used global annual growing-season PDSI data (Palmer 1965; Zhao and Running 2010) were used to evaluate the performance of global annual DSI results. In the PDSI calculation (Palmer 1965; Alley 1984), PET was estimated using Thornthwaite's formula (Thornthwaite 1948). Following Dai et al. (2004), if soil water holding capacity (awc) data from Webb et al. (1993) is no more than 2.54 cm (or 1 in.), then awc is assigned to the top soil layer, and the bottom layer has zero capacity; otherwise, the top layer has 2.54 cm water-holding capacity, while the bottom layer has (awc – 2.54 cm) capacity. The monthly air temperature from NCEP–DOE II (Kanamitsu et al. 2002) was smoothed into half-degree spatial resolution. The monthly half-degree precipitation data generated using the method developed by Chen et al. (2002) based on gauge measurements at weather stations were used instead of data from NCEP–DOE II, since precipitation data from meteorological reanalysis datasets generally contain relatively large uncertainties (Chen

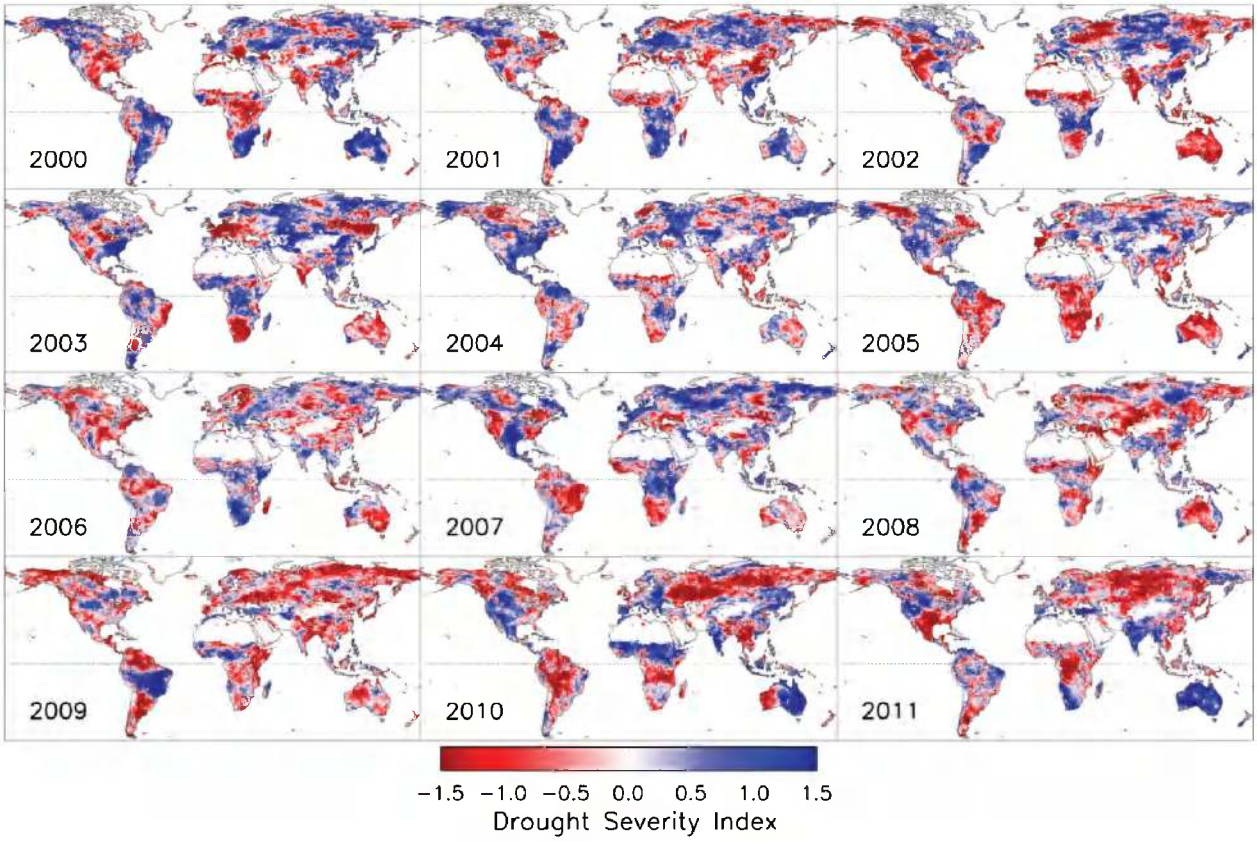

Fig. 1. Annual global terrestrial DSI data over the 2000–11 MODIS record. The DSI ranges theoretically from unlimited negative values to unlimited positive values for dry to wet climate deviations, respectively, from prevailing conditions.

and Bosilovich 2007). For a given month, multiyear average monthly water exchanges were used to quantify the departure level of precipitation (supply) from the normal water demand (Palmer 1965; Dai et al. 2004; Zhao and Running 2010).

RESULTS. We produce the global DSI results at 8-day, monthly, and annual intervals, and 1-km spatial resolution consistent with the MODIS inputs. In this study, we aggregated the 1-km-resolution DSI product into a coarser half-degree-resolution dataset to focus on large-scale droughts.

Annual global DSI. Figure 1 shows the annual global DSI over the 2000–11 MODIS record, which is the period used for defining averages and standard deviations in Eqs. (1)–(5). Negative DSI values represent drier-than-normal conditions and positive values represent relatively wet conditions. We begin our examination of the DSI results in relation to reported droughts within the 2000–11 record.

First, we evaluate DSI performance in the Asia and Pacific region where some 23 million hectares are drought-prone and represent a fifth of the total rice production area of the region (Pandey et al. 2007), and drought represents a major constraint on food production. The high frequency and intensity of droughts in many parts of Asia are captured by the annual DSI (Fig. 1). From 2000 to 2011, vast areas in this region experienced drought (Fig. 1), which affected large tracts of the main rice-producing areas of Asia (6.7 million hectares during 2000–07; Fan et al. 2003; Pandey et al. 2007). In South Asia, consecutive droughts during 2000–03 in Pakistan and northwestern India (Fig. 1) led to sharp declines in water tables and crop failures (Pandey et al. 2007; Fig. 1). In 2004, a severe drought hit Southeast Asia and caused the shriveling of crops on millions of hectares, costing millions of dollars, shortages of water for drinking and irrigation, and the suffering of millions of people (NBS 2005; Fig. 1). In Thailand, the 2004 drought alone (Fig. 1) is estimated to have affected 2 million hectares of cropped area and over 8 million people (Bank of Thailand 2005; *Asia Times,* 29 April 2005).

The DSI captured major documented droughts within the 2000–11 period for North America, where severe drought is purported to be the greatest recurring natural disaster for the region. The continuous severe 1998–2004 drought in the western United States resulted in considerable water supply deficits in reservoir storage (Cook et al. 2007; Fig. 1). When the drought peaked in July 2002, more than 50% of the contiguous United States was under moderate to severe drought conditions, with record or near-record precipitation deficits throughout the West (Lawrimore and Stephens 2003). Large portions of the Canadian prairie provinces also suffered from severe drought (Cook et al. 2007; Fig. 1), as well as extensive areas of Mexico, particularly in the northern and western parts of the country in 2002 (Lawrimore et al. 2002; Fig. 1). The DSI results are also consistent with the severe drought in the contiguous United States in 2006 (Fig. 1) and reported by Dong et al. (2011).

The annual DSI data capture major droughts and floods in Australia (Fig. 1) during the study period. The National Climate Centre (2007) reported a 6-yr widespread drought in southern and eastern Australia from November 2001 to October 2007 (Fig. 1). The 2002–2003 Australia drought (Horridge et al. 2005; Fig. 1) was purported to be one of the worst short-term droughts in Australia's recorded meteorological history (Nicholls 2004). The exceptional drought in 2005 (Watkins 2005) and continuous droughts from 2007 to 2009 in Australia (National Climate Centre 2009) are effectively captured by the annual DSI data (Fig. 1). The period from 2010 to early 2011 experienced one of the strongest La Niña events in history, which caused heavy rain events starting in north and east Australia in spring 2010 and extending across most of Australia into 2011, and resulting in the wettest 2-yr period on record (Fig.1; National Climate Centre 2012).

Several other extreme droughts are captured by the annual DSI in Fig. 1. For example, the DSI results capture the 2003 heat wave in Europe (Ciais et al. 2005; Fig. 1), severe droughts in the Amazon and Africa in 2005 (Hopkin 2005; Phillips et al. 2009; Fig. 1), the Great Russian Heat Wave and severe Amazonian drought in 2010 (Barriopedro et al. 2011; Lewis et al. 2011; Fig. 1), and a severe drought in the Horn of Africa in 2011 (Lyon and Dewitt 2012).

Comparisons between annual DSI and PDSI. The PDSI is a widely used global drought index (Heim 2002; Dai et al. 2004; Wells et al. 2004; Dai 2011a,b). The annual DSI results were therefore evaluated against an alternative global growing-season PDSI dataset (Zhao and Running 2010).

The correlation between the 0.5° annual global terrestrial growing-season PDSI and annual DSI, with an area-weighted average correlation coefficient of 0.43, is shown (Fig. 2). Notably, the correlation between annual DSI and growing-season PDSI (Fig. 2) is the highest where the weather stations are relatively dense, such as in the southeastern United States and

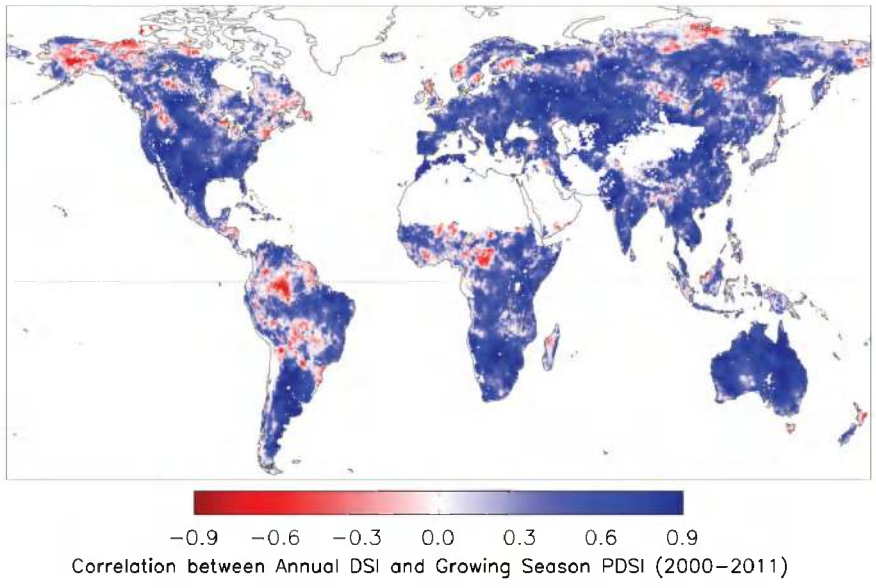

Fig. 2. Spatial correlation coefficient between 12-yr annual global DSI and growing-season PDSI data from 2000 to 2011. The area-weighted average *r* is 0.43 over 36,594 vegetated pixels (~75.8% of the global vegetated domain). The mean correlation is 0.17 for the Amazon, 0.41 in western Europe, and 0.60 in western Russia.

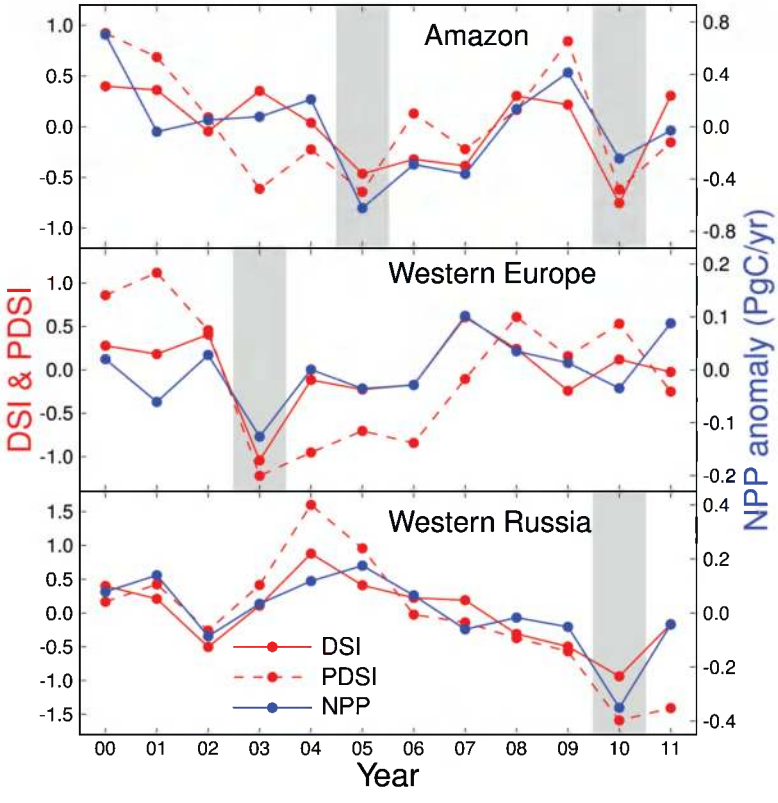

Fig. 3. Annual DSI, growing-season PDSI, and MODIS (MOD17) NPP data for selected subregions, including the Amazon, western Europe, and western Russia regions, and the 2000–11 period. Vertical gray bars denote years with documented droughts within each region.

portions of Eurasia (Fig. 2 in Chen et al. 2002; Fig. 2b in Zhao et al. 2006). The correlation in western Europe (40°–66.5°N, −5°–15°E) is 0.41, and 0.60 in western Russia (40°–66.5°N, 30°–55°E). However, where rain gauges and weather stations are sparse (Fig. 2 in Chen et al. 2002; Fig. 2b in Zhao et al. 2006), the correlation between DSI and PDSI is low, such as middle and northern South America, northern Africa, and the high-latitude areas (Fig. 2). The correlation coefficient in the Amazon [the study region in Lewis et al. (2011)] is only 0.17. This spatial correlation map provides further evidence of uncertainties in the reanalysis data and hence the calculated drought indices, such as PDSI. For example, during the last decade two major drought events—one in 2005 and another in 2010—occurred in the Amazon basin (Atkinson et al. 2011). Xu et al. (2011) suggested that the vegetation browning in 2010 was 4 times greater than in 2005 as a response to the 2010 drought. However, in Fig. 3, the PDSI indicates that 2005 was the driest year (PDSI = −0.644), while 2010 (PDSI = −0.620) and 2003 (PDSI = −0.615) were the second and third driest years of record, respectively, in the Amazon over the 2000–11 period (Figs. 3, 4), which differs from earlier reports (Atkinson et al. 2011; Lewis et al. 2011; Xu et al. 2011).

While comparisons between the DSI and PDSI results provide insight into product performance, both indices have limitations. The various PDSI limitations are described earlier in this paper. A relative advantage of the DSI is that the model integrates remotely sensed ET, PET, and NDVI data to monitor and detect droughts.

Precipitation data are relatively uncertain on a global basis and are not used in the DSI calculation. However, uncertainties in the DSI arise from several other sources, including uncertainties from global reanalysis data inputs (Zhao et al. 2006) and satellite remote sensing inputs into the MODIS ET algorithm, including MODIS FPAR/LAI, land cover (Friedl et al. 2002), and albedo (Schaaf et al. 2002). Other sources of DSI uncertainty are introduced from the MODIS NDVI inputs and the various MODIS ET algorithm assumptions (Mu et al. 2007, 2009, 2011b). Many of the lower correlation areas (Fig. 2), including high-latitude and tropical regions, are also areas where persistent cloud cover, atmospheric aerosols, or low solar illumination significantly constrain satellite optical-IR remote sensing (e.g., Fensholt and Proud 2012); the resulting gaps in the satellite VI retrievals and uncertainty in reanalysis meteorology inputs can degrade the resulting DSI calculations for these areas.

These uncertainties may result in a false DSI drought detection signal. Both the DSI and PDSI show strong negative values in central south China in 2008, such as the Hunan province (Fig. 5); however, the negative drought signal is likely due to a combination of summer drought and damaged trees caused by a preceding severe snow storm and icing event in January 2008 (Zhou et al. 2010). Vegetation activity in southern China is generally not limited by water supply (Nemani et al. 2003). Most of the regional ET flux comes from plant transpiration and evaporation from canopy-intercepted water (figure not shown). The damaged vegetation showed reduced LAI, which lowered plant transpiration and canopy evaporation in the following summer. In the Guangdong province of southern China, the DSI shows a strong negative anomaly in 2008 (Fig. 5a), but the PDSI only shows a weak negative or near-zero value (Fig. 5b). There was no reported drought in the Guangdong province in 2008; the strong negative regional DSI value for this period is likely a false drought signal, though the cause of the negative anomaly is unknown.

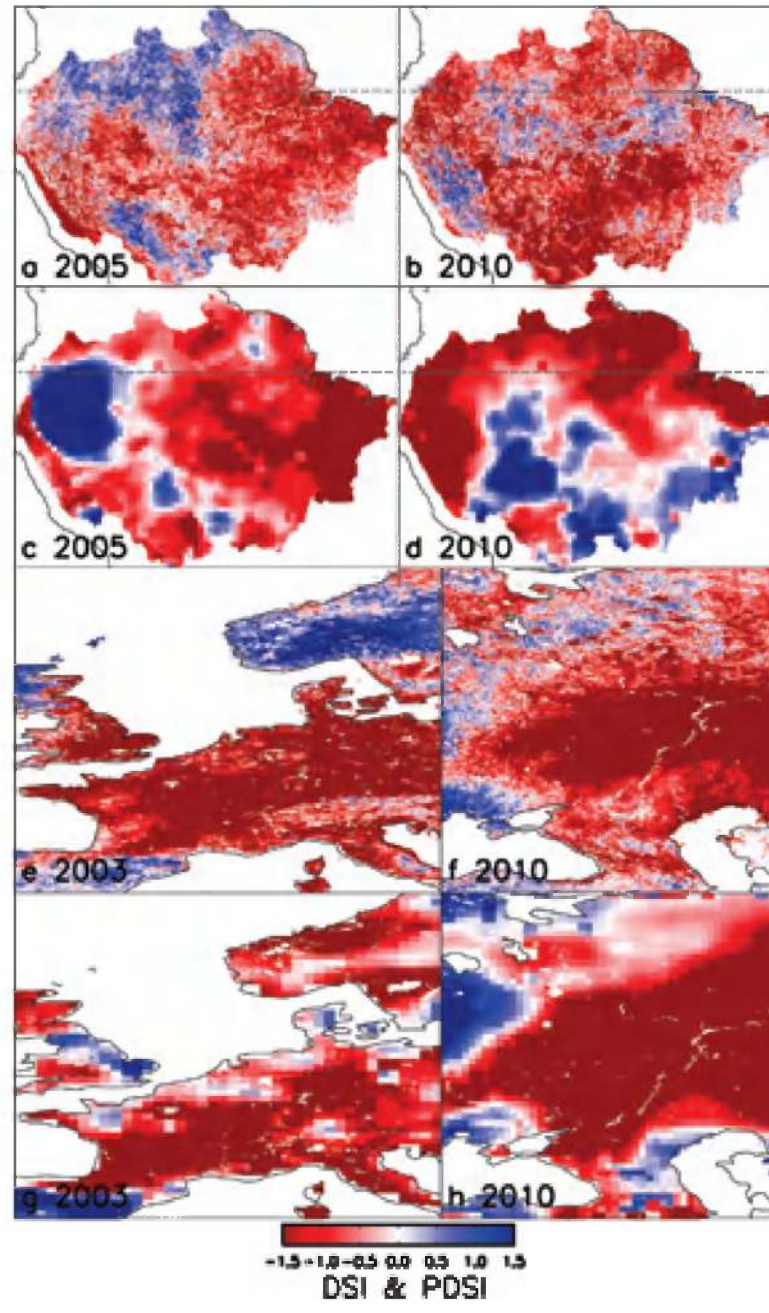

Fig. 4. Spatial patterns of (a),(b),(e),(f) annual DSI and (c),(d),(g),(h) growing-season PDSI for selected subregions, including the Amazon in (a),(c) 2005 and (b),(d) 2010, (e),(g) western Europe in 2003, and (f),(h) western Russia in 2010.

Drought-induced NPP change. We used the MODIS (MOD17) global NPP record as a relative indicator of vegetation productivity changes for comparing against the DSI regional patterns and temporal anomalies. The NPP and DSI results are largely

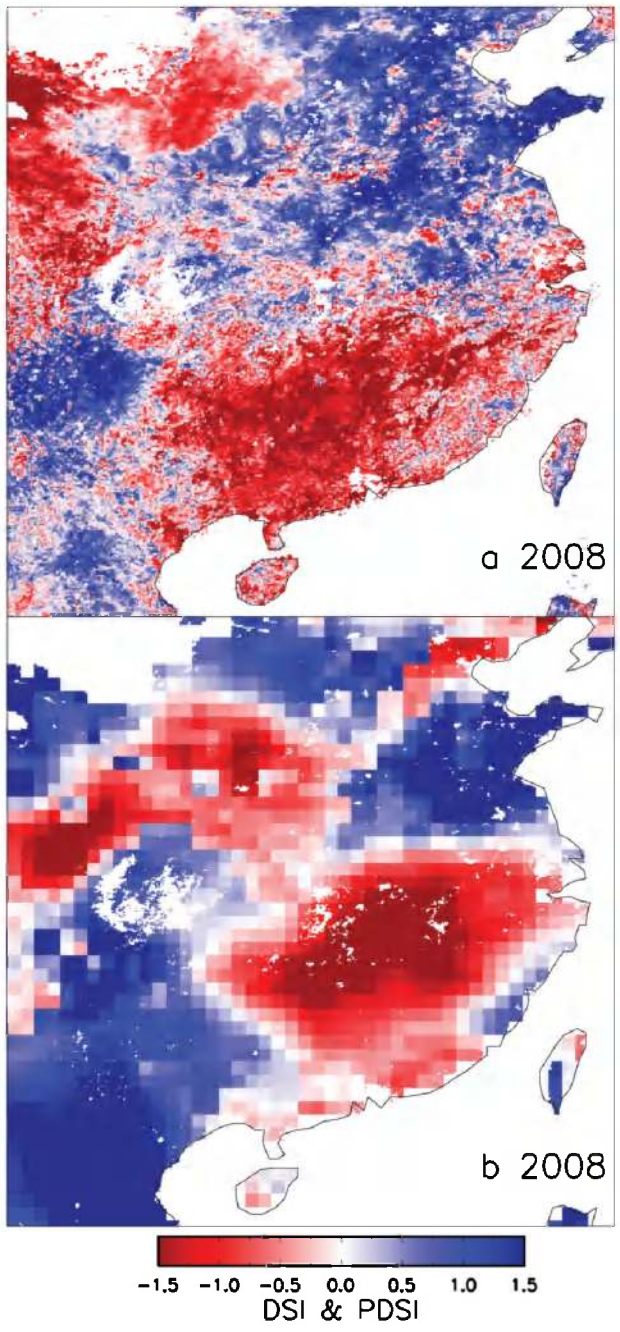

Fig. 5. Spatial patterns of (a) annual DSI and (b) growing-season PDSI over southern China (17.8°–40.8°N, 100°–123°E) in 2008.

independent, but both utilize MODIS dynamic MOD15 LAI/FPAR and reanalysis daily surface meteorology inputs. The DSI and NPP results should be correlated, especially for water supply–constrained regions (Nemani et al. 2003) through vegetation moisture constraints on canopy transpiration, net photosynthesis, and CO_2 exchange. Severe droughts can induce progressive leaf stomatal closure, which reduces plant water loss and photosynthesis. The PDSI and MODIS DSI, ET, and GPP/NPP data were compared to evaluate relationships between DSI- and PDSI-inferred water supply reductions, and associated ecosystem drought responses indicated by the satellite-derived productivity record.

Figure 3 shows the annual DSI, growing-season PDSI, and MODIS NPP results for the Amazon [the region as in Lewis et al. (2011)], western Europe (40°–66.5°N, −5°–15°E), and western Russia (40°–66.5°N, 30°–55°E) from 2000 to 2011. The DSI captures four severe droughts in these regions (Figs. 3, 4) that generally coincide with the other products and are consistent with reported events. In 2003, Europe experienced a severe heat wave (Ciais et al. 2005) that caused 35,000 human deaths (Shaoni 2003). The Amazon rain forest experienced once-in-a-century droughts in 2005 and 2010 (Marengo et al. 2008; Phillips et al. 2009; Atkinson et al. 2011; Lewis et al. 2011; Xu et al. 2011). The Great Russian Heat Wave of 2010 caused extensive wildfires and thousands of human deaths (Barriopedro et al. 2011). Induced by the severe droughts, the NPP record shows anomalous declines in vegetation productivity in all of these dry years, consistent with the DSI results (Fig. 3).

8-day composite global DSI. Drought is a progressive lack of water in an area usually over a time scale of a month or longer. However, weekly- or 8-day information is still critical for near-real-time drought monitoring, especially for areas with consecutive multi-8-day drought. The finer (8 days) DSI temporal fidelity provides potentially greater precision for documenting drought onset, duration, and transient wetting/drying events, but it should be used with caution because of reduced signal-to-noise ratio for distinguishing climatological drought from variable weather. Both small and large-scale drought patterns can be clearly identified in the 8-day composite global DSI maps in 2011. For example, early spring drought occurred over large areas of northern Eurasia, followed by early summer drought. Persistent drought in Texas and surrounding areas of the United States, and the Horn of Africa are also clearly depicted (not shown). The 2011 drought in the Horn of Africa was caused by a failure of the East African rains (March–May) in spring 2011, consistent with a recurrent large-scale precipitation pattern that followed their abrupt decline around 1999 (Lyon and Dewitt 2012).

Classification of drought severity index. The DSI provides a measure of wetness relative to normal, which is proposed in this study to monitor and display the magnitude and spatial extent of drought

Table 2. Dynamic range and relative categories for wet (W) and dry (D) conditions of the global PDSI and DSI.							
Category	Description	PDSI	DSI	Category	Description	PDSI	DSI
W5	Extremely wet	4.00 or greater	1.5 or greater	D1	Incipient drought	−0.50 to −0.99	−0.3 to −0.59
W4	Very wet	3.00 to 3.99	1.2 to 1.49	D2	Mild drought	−1.00 to −1.99	−0.6 to −0.89
W3	Moderately wet	2.00 to 2.99	0.9 to 1.19	D3	Moderate drought	−2.00 to −2.99	−0.9 to −1.19
W2	Slightly wet	1.00 to 1.99	0.6 to 0.89	D4	Severe drought	−3.00 to −3.99	−1.2 to −1.49
W1	Incipient wet spell	0.50 to 0.99	0.3 to 0.59	D5	Extreme drought	−4.00 or less	−1.5 or less
WD	Near normal	0.49 to −0.49	0.29 to −0.29				

over the global terrestrial land surface. For consistency, we scaled the DSI classification levels to the corresponding PDSI drought severity categories, where D1–5 and W1–5 categories denote progressively drier and wetter conditions, respectively (Palmer 1965; Table 2). While the primary objective of this study is drought detection, the DSI (and PDSI) can also detect abnormally wet periods.

DISCUSSION. There have been 12 yr of MODIS ET and NDVI data, enabling a continuous global DSI record from 2000 to 2011, with the potential for continued operations. The DSI appears to capture the major regional droughts that have been reported over the last decade (e.g., Figs. 1, 3, 4). The World Meteorological Organization, the National Oceanic and Atmospheric Administration, and the National Aeronautics and Space Administration all reported that the last decade of the twenty-first century was the warmest decade since instrumental measurements of temperatures began in the 1880s (Zhao and Running 2010; Mu et al. 2011a). Under a warming climate, drought severity and persistence may increase (Dai et al. 2004; Dai 2011b).

The 12-yr record used in this study may be too short to characterize "normal" climatological conditions required for accurate DSI drought detection and monitoring. We conducted a sensitivity study to examine how the base period length affects the DSI results, by varying the base period length over 6-yr (2000–05; 6yr_std), 7-yr (2000–06; 7yr_std), 8-yr (2000–07; 8yr_std), 9-yr (2000–08; 9yr_std), 10-yr (2000–09; 10yr_std), 11-yr (2000–10; 11yr_std), and 12-yr (2000–11; 12yr_std) periods. Also, to test the uncertainties in the DSI product induced by the input global meteorological reanalysis data to the MODIS ET/PET algorithm, we used an alternative [Global Modeling and Assimilation Office Modern Era Retrospective-Analysis for Research and Applications (GMAO MERRA)] global reanalysis dataset with approximately 0.5° spatial resolution (Yi et al. 2011) as meteorological input data to the MODIS ET/PET algorithm to estimate global 1-km MODIS ET/PET, and hence global annual DSI with the base period of 2000–11. We then integrated the global 1-km annual DSI data from the different experiments into a consistent 0.5° resolution, and calculated the area-weighted spatial correlation coefficients between these different experiments and the 12yr_std DSI baseline for each year (Fig. 6). The resulting correlation is significant for each year in each experiment over the 36,594 0.5° vegetated

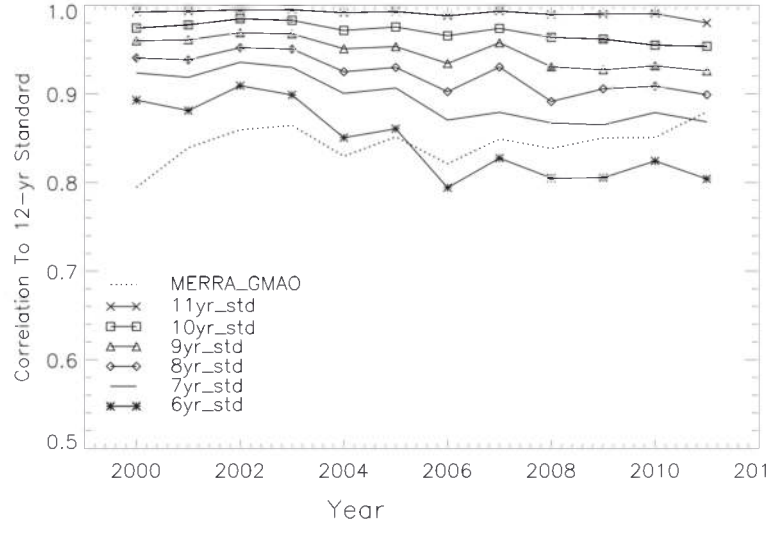

Fig. 6. Area-weighted annual spatial correlation coefficients between 12yr_std (baseline) global DSI data and alternative global DSI calculations determined from different sensitivity and uncertainty experiments involving progressively shorter record lengths for determining normal DSI conditions ranging from 6-yr (6yr_std) to 11-yr (11yr_std) periods, and alternative DSI calculations derived from GMAO MERRA (MERRA_GMAO) reanalysis inputs.

pixels. The spatial patterns of global DSI results from the different sensitivity experiments using different base period lengths are very close (not shown), though some differences occur over small areas, and the degree of drought from the 6yr_std experiment may be different from the 12yr_std baseline. When there are at least eight years of MODIS ET/PET and NDVI data, the global DSI product does not change significantly over longer base period lengths.

For the uncertainty experiment driven by GMAO MERRA meteorological data, though there are substantial differences between the GMAO and NCEP–DOE II (Kanamitsu et al. 2002) reanalysis datasets, the area-weighted spatial correlation coefficients between the resulting DSI calculations are significant over the 36,594 global vegetated pixels (Fig. 6), and the spatial patterns of the 12-yr annual global DSI results are very close to those driven by NCEP–DOE II reanalysis data (figures not shown). To reduce the DSI uncertainties caused by using a single reanalysis dataset, we suggest that future applications only label a region as undergoing drought when both the DSI using MODIS ET/PET driven by MERRA GMAO and NCEP–DOE II reanalysis datasets detect drought. In the future, not only PDSI but also other widely used drought indices, such as SPI and PNP, and more historical drought and flooding cases will be used to validate and improve the DSI product.

FUTURE STUDIES AND ANTICIPATED IMPACTS. The operational production of similar vegetation indices from the Visible Infrared Imaging Radiometer Suite (VIIRS) on the National Polar-orbiting Operational Environmental Satellite System (NPOESS) Preparatory Project and Joint Polar Satellite System (JPSS) satellites enables the potential continuation of global DSI and ET records in the post–EOS MODIS era. We suggest additional follow-up studies to clarify the DSI's utility and limitations, and to improve understanding of drought globally. First, the DSI should be evaluated against extensive historic climate records to clarify further product sensitivity and the range and diversity of ecosystem responses to drought. Evaluation of the DSI and its associated input parameters (ET, PET, NDVI) against long-term ET observations from the flux network (FLUXNET; Baldocchi 2008) will allow improved understanding of DSI performance and limitations. Regional comparisons of alternative drought monitoring methods, including the DSI, against a range of observations provides a means for better understanding of relationships and limitations among the various approaches, which may lead to further improvements in product accuracy and utility. The global terrestrial DSI product from this study is available online for public use (ftp://ftp.ntsg.umt.edu/pub/MODIS/Mirror/DSI) and provides a potential means for global assessment and potential monitoring of drought occurrence, severity, and duration at relatively fine (1-km resolution) spatial scales. The DSI and similar global products derived from operational satellite remote sensing should be useful for regional drought assessment and mitigation efforts, especially for areas of the globe where sparse measurement networks and poor infrastructure development limit other information sources.

ACKNOWLEDGMENTS. This work is funded by the NASA Earth Observing System MODIS project (Grant NNH09ZDA001N-TERRA-AQUA). We thank the anonymous reviewers, as well as communications with Dr. Michael J. Hayes at the University of Nebraska at Lincoln. The shapefile for Amazon is provided by Dr. Simon L. Lewis.

REFERENCES

Alley, W. M., 1984: The Palmer drought severity index: Limitations and assumptions. *J. Climate Appl. Meteor.*, **23,** 1100–1109.

Atkinson, P. M., J. Dash, and C. Jeganathan, 2011: Amazon vegetation greenness as measured by satellite sensors over the last decade. *Geophys. Res. Lett.*, **38,** L19105, doi:10.1029/2011GL049118.

Baldocchi, D. D., 2008: "Breathing" of the terrestrial biosphere: Lessons learned from a global network of carbon dioxide flux measurement systems. *Aust. J. Bot.*, **56,** 1–26.

Bank of Thailand, 2005: The inflation report: January 2005. Bank of Thailand Rep., 97 pp. [Available online at www.bot.or.th/English/MonetaryPolicy/Inflation/Download/Doc_LibInflation%20Report/5.1.1full_eng.pdf.]

Barriopedro, D., E. M. Fischer, J. Luterbacher, R. M. Trigo, and R. García-Herrera, 2011: The hot summer of 2010: Redrawing the temperature record map of Europe. *Science,* **332,** 220–224.

Bouchet, R. J., 1963: Evapotranspiration réelle et potentielle signification climatique. IASH Publ. 62, 134–142.

Chen, J., and M. G. Bosilovich, 2007: Hydrological variability and trends in global reanalyses. Preprints, *19th Conf. on Climate Variability and Change,* San Antonio, TX, Amer. Meteor. Soc., JP4.3. [Available online at https://ams.confex.com/ams/87ANNUAL/techprogram/paper_119754.htm.]

Chen, M., P. Xie, J. E. Janowiak, and P. A. Arkin, 2002: Global land precipitation: A 50-yr monthly analysis based on gauge observations. *J. Hydrometeor.,* **3,** 249–266.

Ciais, Ph., and Coauthors, 2005: Europe-wide reduction in primary productivity caused by the heat and drought in 2003. *Nature,* **437,** 529–533.

Cook, E. R., R. Seager, M. A. Cane, and D. W. Stahle, 2007: North American drought: Reconstructions, causes, and consequences. *Earth-Sci. Rev.,* **81,** 93–134.

Courault, D., B. Seguin, and A. Olioso, 2005: Review on estimation of evapotranspiration from remote sensing data: From empirical to numerical modeling approaches. *Irrig. Drain. Syst.,* **19,** 223–249.

Dai, A., 2011a: Characteristics and trends in various forms of the Palmer drought severity index during 1900–2008. *J. Geophys. Res.,* **116,** D12115, doi:10.1029/2010JD015541.

——, 2011b: Drought under global warming: A review. *Wiley Interdiscip. Rev. Climate Change,* **2,** 45–65.

——, K. E. Trenberth, and T. Qian, 2004: A global dataset of Palmer drought severity index for 1870–2002: Relationship with soil moisture and effects of surface warming. *J. Hydrometeor.,* **5,** 1117–1130.

Doesken, N. J., T. B. McKee, and J. D. Kleist, 1991: Development of a surface water supply index for the western United States: Final report. Climatology Rep. 91-3, Colorado State University, 76 pp.

Dong, X., and Coauthors, 2011: Investigation of the 2006 drought and 2007 flood extremes at the Southern Great Plains through an integrative analysis of observations. *J. Geophys. Res.,* **116,** D03204, doi:10.1029/2010JD014776.

Douglas, O. F., and S. D. Prince, 1996: Rainfall and foliar dynamics in tropical southern Africa: Potential impacts of global climate change on savanna vegetation. *Climatic Change,* **33,** 69–96.

Fan, S., C. Chan-Kang, K. Qian, and K. Krishnaiah, 2003: National and international agricultural research and rural poverty: The case of rice in India and China. EPTD Discussion Paper 109, International Food Policy Research Institute, 35 pp.

Fensholt, R., and S. R. Proud, 2012: Evaluation of earth observation based global long term vegetation trends—Comparing GIMMS and MODIS global NDVI time series. *Remote Sens. Environ.,* **119,** 131–147.

Fisher, J. B., K. Tu, and D. D. Baldocchi, 2008: Global estimates of the land–atmosphere water flux based on monthly AVHRR and ISLSCP-II data, validated at FLUXNET sites. *Remote Sens. Environ.,* **112,** 901–919.

Friedl, M. A., and Coauthors, 2002: Global land cover mapping from MODIS: Algorithms and early results. *Remote Sens. Environ.,* **83,** 287–302.

Gao, H., Q. Tang, C. R. Ferguson, E. F. Wood, and D. P. Lettenmaier, 2010: Estimating the water budget of major U.S. river basins via remote sensing. *Int. J. Remote Sensing,* **31,** 3955–3978.

Gibbs, W. J., and J. V. Maher, 1967: *Rainfall Deciles as Drought Indicators.* Bureau of Meteorology Bulletin, No. 48, Commonwealth of Australia, 33 pp.

Hall, D. K., and G. A. Riggs, 2007: Accuracy assessment of the MODIS snow products. *Hydrol. Processes,* **21,** 1534–1547.

Heim, R. R., Jr., 2002: A review of twentieth-century drought indices used in the United States. *Bull. Amer. Meteor. Soc.,* **83,** 1149–1165.

Heinsch, F. A., and Coauthors, 2006: Evaluation of remote sensing based terrestrial productivity from MODIS using regional tower eddy flux network observations. *IEEE Trans. Geosci. Remote Sensing,* **44,** 1908–1925.

Hopkin, M., 2005: Amazon hit by worst drought for 40 years: Warming Atlantic linked to both US hurricanes and rainforest drought. *Nature News*, doi: 10.1038/news051010-8.

Horridge, M., J. Madden, and G. Wittwer, 2005: The impact of the 2002–2003 drought on Australia. *J. Policy Model.,* **27,** 285–308.

Huete, A., K. Didan, T. Miura, E. P. Rodriguez, X. Gao, and L. G. Ferreira, 2002: Overview of the radiometric and biophysical performance of the MODIS vegetation indices. *Remote Sens. Environ.,* **83,** 195–213.

Jiang, L., S. Islam, and T. Carlson, 2004: Uncertainties in latent heat flux measurement and estimation: Implications for using a simplified approach with remote sensing data. *Can. J. Remote Sensing,* **30,** 769–787.

Jung, M., and Coauthors, 2010: Recent decline in the global land evapotranspiration trend due to limited moisture supply. *Nature,* **467,** 951–954.

Justice, C. O., J. R. G. Townshend, E. F. Vermote, E. Masuoka, R. E. Wolfe, N. Saleous, D. P. Roy, and J. T. Morisette, 2002: An overview of MODIS Land data processing and product status. *Remote Sens. Environ.,* **83,** 3–15.

Kalma, J. D., T. R. McVicar, and M. F. McCabe, 2008: Estimating land surface evaporation: A review of methods using remotely sensed surface temperature data. *Surv. Geophys.,* **29,** 421–469.

Kanamitsu, M., W. Ebisuzaki, J. Woollen, S.-K. Yang, J. J. Hnilo, M. Fiorino, and G. L. Potter, 2002: NCEP–DOE AMIP-II Reanalysis (R-2). *Bull. Amer. Meteor. Soc.,* **83,** 1631–1643.

Kerr, R. A., 2011: Vital details of global warming are eluding forecasters. *Science,* **334,** 173–174.

Keyantash, J., and J. A. Dracup, 2002: The quantification of drought: An evaluation of drought indices. *Bull. Amer. Meteor. Soc.,* **83,** 1167–1180.

Lawrimore, J., and S. Stephens, 2003: Climate of 2002 annual review. NOAA National Climatic Data Center. [Available online at http://lwf.ncdc.noaa.gov/oa/climate/research/2002/ann/events.html.]

——, R. R. Heim Jr., M. Svoboda, V. Swail, and P. J. Englehart, 2002: Beginning a new era of drought monitoring across North America. *Bull. Amer. Meteor. Soc.,* **83,** 1191–1192.

Lewis, S. L., P. M. Brando, O. L. Phillips, G. M. F. van der Heijden, and D. Nepstad, 2011: The 2010 Amazon drought. *Science,* **331,** 554.

Loarie, S. R., D. B. Lobell, G. P. Asner, Q. Mu, and C. B. Field, 2011: Direct impacts on local climate of expanding sugarcane in Brazil. *Nat. Climate Change,* **1,** 105–109.

Los, S. O., and Coauthors 2000: A global 9-yr biophysical land surface dataset from NOAA AVHRR data. *J. Hydrometeor.,* **1,** 183–199.

Lyon, B., and D. G. DeWitt, 2012: A recent and abrupt decline in the East African long rains. *Geophys. Res. Lett.,* **39,** L02702, doi:10.1029/2011GL050337.

Marengo, J. A., and Coauthors, 2008: The drought of Amazonia in 2005. *J. Climate,* **21,** 495–516.

McKee, T. B., N. J. Doesken, and J. Kleist, 1993: The relationship of drought frequency and duration to time scales. Preprints, *Eighth Conf. on Applied Climatology,* Anaheim, CA, Amer. Meteor. Soc., 179–184.

Meehl, G. A., and Coauthors, 2007: Global climate projections. *Climate Change 2007: The Physical Science Basis,* S. Solomon et al., Eds., Cambridge University Press, 747–845.

Monteith, J. L., 1965: Evaporation and environment. *The State and Movement of Water in Living Organisms,* G. E. Fogg, Ed., Symposia of the Society for Experimental Biology, Vol. 19, Academic Press, 205–234.

Montenegro, A., M. Eby, Q. Mu, M. Mulligan, A. J. Weaver, E. C. Wiebe, and M. Zhao, 2009: The net carbon drawdown of small scale afforestation from satellite observations. *Global Planet. Change,* **69,** 195–204.

Mu, Q., F. A. Heinsch, M. Zhao, and S. W. Running, 2007: Development of a global evapotranspiration algorithm based on MODIS and global meteorology data. *Remote Sensing Environ.,* **111,** 519–536.

——, L. A. Jones, J. S. Kimball, K. C. McDonald, and S. W. Running, 2009: Satellite assessment of land surface evapotranspiration for the pan-Arctic domain. *Water Resour. Res.,* **45,** W09420, doi:10.1029/2008WR007189.

——, M. Zhao, and S. W. Running, 2011a: Evolution of hydrological and carbon cycles under a changing climate. Part III: Global change impacts on landscape scale evapotranspiration. *Hydrol. Processes,* **25,** 4093–4102.

——, ——, and ——, 2011b: Improvements to a MODIS global terrestrial evapotranspiration algorithm. *Remote Sensing Environ.,* **115,** 1781–1800.

Myneni, R. B., and Coauthors, 2002: Global products of vegetation leaf area and fraction absorbed PAR from year one of MODIS data. *Remote Sensing Environ.,* **83,** 214–231.

Narasimhan, B., and R. Srinivasan, 2005: Development and evaluation of soil moisture deficit index (SMDI) and evapotranspiration deficit index (ETDI) for agricultural drought monitoring. *Agric. Forest Meteor.,* **133,** 69–88.

National Climate Centre, 2007: Six years of widespread drought in southern and eastern Australia: November 2001–October 2007. Bureau of Meteorology Special Climate Statement 14, 6 pp.

——, 2009: A prolonged spring heatwave over central and south-eastern Australia. Bureau of Meteorology Special Climate Statement 19, 15 pp.

——, 2012: Australia's wettest two-year period on record; 2010–2011: Bureau of Meteorology Special Climate Statement 38, 10 pp.

NBS, 2005: *China Statistical Yearbook 2004.* National Bureau of Statistics of China, 1011 pp. [Available online at www.stats.gov.cn/english/statisticaldata/yearlydata/.]

Nemani, R. R., C. D. Keeling, H. Hashimoto, W. M. Jolly, S. C. Piper, C. J. Tucker, R. B. Myneni, and S. W. Running, 2003: Climate-driven increases in global terrestrial net primary production from 1982 to 1999. *Science,* **300,** 1560–1563.

Nicholls, N., 2004: The changing nature of Australian droughts. *Climatic Change,* **63,** 323–336.

Nicholson, S. E., C. J. Tucker, and M. B. Ba, 1998: Desertification, drought, and surface vegetation: An example from the West African Sahel. *Bull. Amer. Meteor. Soc.,* **79,** 815–829.

Oki, T., and S. Kanae, 2006: Global hydrological cycles and world water resources. *Science,* **313,** 1068–1072.

Pachauri, R. K., and A. Reisinger, Eds., 2007: *Climate Change 2007: Synthesis Report.* Cambridge University Press, 104 pp.

Palmer, W. C., 1965: Meteorological drought. U.S. Weather Bureau Research Paper 45, 65 pp.

——, 1968: Keeping track of crop moisture conditions, nationwide: The new crop moisture index. *Weatherwise,* **21,** 156–161.

Pandey, S., H. N. Bhandari, and B. Hardy, 2007: Economic costs of drought and rice farmers' coping mechanisms: A cross-country comparative analysis. IRRI Rep., 203 pp.

Paruelo, J. M., and W. K. Lauenroth, 1995: Regional pattern of normalized difference vegetation index in North American shrublands and grasslands. *Ecology,* **76,** 1888–1898.

Phillips, O. L., and Coauthors, 2009: Drought sensitivity of the Amazon rainforest. *Science,* **323,** 1344–1347.

Priestley, C. H. B., and R. J. Taylor, 1972: On the assessment of surface heat flux and evaporation using large-scale parameters. *Mon. Wea. Rev.,* **100,** 81–92.

Rosegrant, M. W., X. Cai, and S. A. Cline, 2003: Will the world run dry? Global water and food security. *Environment,* **45,** 24–36.

Running, S. W., R. R. Nemani, F. A. Heinsch, M. Zhao, M. C. Reeves, and H. Hashimoto, 2004: A continuous satellite-derived measure of global terrestrial primary production. *BioScience,* **54,** 547–560.

Schaaf, C. B., and Coauthors, 2002: First operational BRDF, albedo nadir reflectance products from MODIS. *Remote Sens. Environ.,* **83,** 135–148.

Schultz, P. A., and M. S. Halpert, 1995: Global analysis of the relationships among a vegetation index, precipitation, and land surface temperature. *Int. J. Remote Sens.,* **16,** 2755–2777.

Shafer, B. A., and L. E. Dezman, 1982: Development of a surface water supply index (SWSI) to assess the severity of drought conditions in snowpack runoff areas. *Proc. 50th Annual Western Snow Conf.,* Reno, NV, Western Snow Conference, 164–175.

Shaoni, B., 2003: European heatwave caused 35,000 deaths. [Available online at www.newscientist.com/article/dn4259-european-heatwavecaused-35000-deaths.html.]

Svoboda, M., and Coauthors, 2002: The drought monitor. *Bull. Amer. Meteor. Soc.,* **83,** 1181–1190.

Thornthwaite, C. W., 1948: An approach toward a rational classification of climate. *Geogr. Rev.,* **38,** 55–94.

Trenberth, K. E., and Coauthors, 2007: Observations: Surface and atmospheric climate change. *Climate Change 2007: The Physical Science Basis,* S. Solomon et al., Eds., Cambridge University Press, 235–236.

Tsakiris, G., and H. Vangelis, 2005: Establishing a drought index incorporating evapotranspiration. *Eur. Water,* **9–10,** 3–11.

——, D. Pangalou, and H. Vangelis, 2007: Regional drought assessment based on the reconnaissance drought index (RDI). *Water Resour. Manage.,* **21,** 821–833.

Tucker, C. J., 1979: Red and photographic infrared linear combinations for monitoring vegetation. *Remote Sensing Environ.,* **8,** 127–150.

Turner, D. P., and Coauthors, 2005: Site-level evaluation of satellite-based global terrestrial gross primary production and net primary production monitoring. *Global Change Biol.,* **11,** 666–684.

——, and Coauthors, 2006: Evaluation of MODIS NPP and GPP products across multiple biomes. *Remote Sens. Environ.,* **102,** 282–292.

Vermote, E., and S. Kotchenova, 2010: MODIS directional surface reflectance product: Method, error estimates and validation. *Land Remote Sensing and Global Environmental Change: NASA's Earth Observing System and the Science of ASTER and MODIS,* B. Ramachandran, C. O. Justice, and M. J. Abrams, Eds., Remote Sensing and Digital Image Processing Series, Vol. 11, Springer, 533–548.

Vörösmarty, C. J., and Coauthors, 2010: Global threats to human water security and river biodiversity. *Nature,* **467,** 555–561.

Watkins, A. B., 2005: The Australian drought of 2005. [Available online at www.geo.uio.no/edc/downloads/the_australian_drought_of_2005_-_offprint_of_wmo_bulletin_2005_54(3)_156-162.pdf.]

Webb, R. S., C. E. Rosenzweig, and E. R. Levine, 1993: Specifying land surface characteristics in general circulation models: Soil profile data set and derived water-holding capacities. *Global Biogeochem. Cycles,* **7,** 97–108.

Wells, N., S. Goddard, and M. J. Hayes, 2004: A self-calibrating Palmer drought severity index. *J. Climate,* **17,** 2335–2351.

Werick, W. J., G. E. Willeke, N. B. Guttman, J. R. M. Hosking, and J. R. Wallis, 1994: National drought atlas developed. *Eos, Trans. Amer. Geophys. Union,* **75,** 89.

Wilhite, D. A., and M. H. Glantz, 1985: Understanding the drought phenomenon: The role of definitions. *Water Int.,* **10,** 111–120.

Wood, E. F., and Coauthors, 2011: Hyperresolution global land surface modeling: Meeting a grand challenge for monitoring Earth's terrestrial water. *Water Resour. Res.,* **47,** W05301, doi:10.1029/2010WR010090.

Xu, L., A. Samanta, M. H. Costa, S. Ganguly, R. R. Nemani, and R. B. Myneni, 2011: Widespread decline in greenness of Amazonian vegetation due to the 2010 drought. *Geophys. Res. Lett.,* **38,** L07402, doi:10.1029/2011GL046824.

Yao, Y., S. Liang, Q. Qin, and K. Wang, 2010: Monitoring drought over the conterminous United States using MODIS and NCEP Reanalysis-2 data. *J. Appl. Meteor. Climatol.,* **49,** 1665–1680.

Yi, Y., J. S. Kimball, L. A. Jones, R. Reichle, and K. C. McDonald, 2011: Evaluation of MERRA land surface estimates in preparation for the Soil Moisture Active Passive Mission. *J. Climate,* **24,** 3797–3816.

Zhao, M., and S. W. Running, 2010: Drought-induced reduction in global terrestrial net primary production from 2000 through 2009. *Science,* **329,** 940–943.

——, and ——, 2011: Response to comments on "Drought-induced reduction in global terrestrial net primary production from 2000 through 2009." *Science,* **333,** 1093.

——, F. A. Heinsch, R. Nemani, and S. W. Running, 2005: Improvements of the MODIS terrestrial gross and net primary production global data set. *Remote Sens. Environ.,* **95,** 164–176.

——, S. W. Running, and R. R. Nemani, 2006: Sensitivity of Moderate Resolution Imaging Spectroradiometer (MODIS) terrestrial primary production to the accuracy of meteorological reanalyses. *J. Geophys. Res.,* **111,** G01002, doi:10.1029/2004JG000004.

Zhou, B., and Coauthors, 2010: The Great 2008 Chinese Ice Storm: Its socioeconomic–ecological impact and sustainability lessons learned. *Bull. Amer. Meteor. Soc.,* **92,** 47–60.